PHYSICAL REVIEW FLUIDS **1**, 051201(R) (2016)

Resonant alignment of microswimmer trajectories in oscillatory shear flows

Alexander Hope,[1] Ottavio A. Croze,[2,*] Wilson C. K. Poon,[3] Martin A. Bees,[4] and Mark D. Haw[1]

[1]*Department of Chemical and Process Engineering, University of Strathclyde, 75 Montrose Street, Glasgow G1 1XJ, United Kingdom*

[2]*Cavendish Laboratory, University of Cambridge, Cambridge CB3 0HE, United Kingdom*

[3]*SUPA and The School of Physics & Astronomy, The University of Edinburgh, Mayfield Road, Edinburgh EH9 3JZ, United Kingdom*

[4]*Department of Mathematics, University of York, York YO10 5DD, United Kingdom*

(Received 12 January 2016; published 20 September 2016)

Oscillatory flows are commonly experienced by swimming micro-organisms in the environment, industrial applications, and rheological investigations. We characterize experimentally the response of the alga *Dunaliella salina* to oscillatory shear flows and report the surprising discovery that algal swimming trajectories orient perpendicular to the flow-shear plane. The ordering has the characteristics of a resonance in the driving parameter space. The behavior is qualitatively reproduced by a simple model and simulations accounting for helical swimming, suggesting a mechanism for ordering and criteria for the resonant amplitude and frequency. The implications of this work for active oscillatory rheology and industrial algal processing are discussed.

DOI: 10.1103/PhysRevFluids.1.051201

Introduction. Many swimming micro-organisms experience shear flow in natural and industrial processes. Swimming is strongly biased by environmental cues and fluid shear [1,2], with significant implications for ecology [3] and industrial exploitation [4]. Classic examples include directed swimming relative to light (phototaxis) and hydrodynamic focusing in downwelling flow due to viscous and gravitational torques (gyrotaxis) [1,5].

There is great potential to use individual and collective microswimmer behavior to improve microbial biotechnology, such as algal photobioreactor design [4]. For example, gyrotactic micro-organisms in laminar channel flow tend to focus and so drift faster and diffuse less than nonswimming cells or nutrients [6,7], while in turbulent flows cells accumulate in transiently downwelling [7–9] or strongly accelerated [10] regions. Horizontal shear flows can trap gyrotactic swimmers (a mechanism for oceanic thin layers) [3] and modify hydrodynamic instabilities and patterns (bioconvection) [11,12]. Phototaxis and shear flow can combine to drive cell focusing [13] and pattern formation [14]. Complex transport dynamics can even result from relatively simple shear flow [2,15]. The rheology of active media is also of recent interest: Suspensions of swimming bacteria behave less viscously [16] and algae more viscously [17] than dead cells.

Here we investigate the interaction of the swimming alga *Dunaliella salina* with oscillatory shear flows. Surprisingly, in experiments swimming trajectories are strongly ordered by the flow for particular driving parameter values. The ordering mechanism is distinct from that observed recently with *Dunaliella primolecta*, with constant, strong shear flows [18]. We explore the observed resonant ordering employing simple but predictive models and discuss implications for active oscillatory rheology and industrial processing of swimming algae.

Experiment. D. salina CCAP (culture collection of algae and protozoa) 19/18 cells (long axis $\approx 15\,\mu$m) were grown on a modified Pick medium [19,20] under a 12:12 light-dark cycle at 21 °C. All experiments were carried out at this temperature. Cells were concentrated by upswimming (gravitaxis) using cotton wool rafts [11]. Dilute (10^6 cells/ml) suspensions were subjected to

*oac24@cam.ac.uk

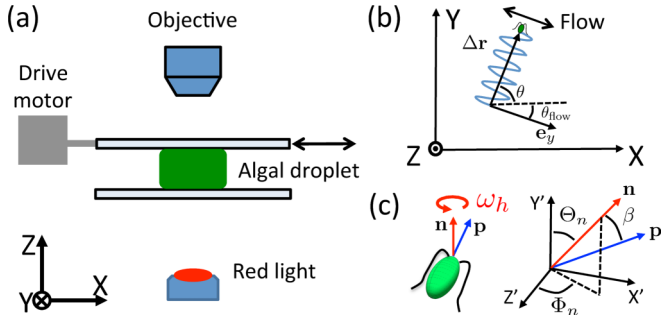

FIG. 1. (a) Oscillatory flow and imaging setup. (b) Trajectory orientations θ from the x axis are evaluated from their displacements $\Delta\mathbf{r}$. The flow axis $\mathbf{e}_y$ was often rotated by θ_{flow} from x (consistent across repeat experiments). (c) Shown on the left are *Dunaliella salina* swimming and helical rotation directions $\mathbf{p}$ and $\mathbf{n}$ and on the right model coordinate system and angles (see the text).

oscillatory shear on the stage of an optical microscope (Olympus BX51). The suspension was placed between two transparent parallel plates 400 μm apart, the top plate connected to an electromechanical drive that sinusoidally sheared the suspension (Fig. 1). Plate parallelism was ensured by zeroing sample capillary flow. Video sequences (100–400 Hz) of sheared algae were acquired using a Mikrotron MC1310 at 10× (numerical aperture 0.25) using red-filtered bright-field illumination to minimize phototaxis [21]. Sequences were captured in a plane equidistant from top and bottom plates at a depth of 200 μm. Algae were tracked using MATLAB versions of established algorithms [22,23]. The direction of the imposed oscillating flow was inferred from short-time cell trajectories and confirmed by tracking PEGylated polystyrene colloids [24]. Cell observation before and after measurements found that the apparatus did not damage the cells (e.g., deflagellation).

With no flow, *D. salina* swimming trajectories were distributed isotropically in the horizontal plane [Fig. 2(a)]. As in Ref. [25], gravitactic bias was not evident for tracks in this plane on experimental time scales. On application of oscillatory shear with amplitude A and frequency f trajectories might be expected simply to reflect superposition of isotropic swimming and oscillatory advection. This was indeed the case for some driving parameters, such as $A = 240\ \mu$m and $f = 6$ Hz [Fig. 2(b)]. However, for $A = 448\ \mu$m and $f = 2$ Hz swimming trajectories unexpectedly aligned perpendicular to the flow-shear plane [Fig. 2(c)]. Alignment can be quantified by the start-to-end displacement $\Delta\mathbf{r}(\tau)$ of each swimmer trajectory [Fig. 1(b)]. Evaluated at short times within a cycle, $\Delta\mathbf{r}(\tau)$ provides the flow direction $\mathbf{e}_y \sim \Delta\mathbf{r}(\tau \to 0)$. However, evaluating $\Delta\mathbf{r}(\tau)$ over the largest available integer multiple n of the oscillation period $\tau = n/f$ provides overall trajectory orientation θ and speed $v_t = |\Delta\mathbf{r}|/\tau$.

Distributions $P(\theta)$ of orientations are presented beside the trajectories in Fig. 2. The distribution for $f = 2$ Hz and $A = 448\ \mu$m shows how trajectories orient along the line perpendicular to the flow-shear plane, but are equally likely in either direction along this line. If the flow is halted, the distribution returns to uniform [24]. Speed distributions for aligned trajectories [Fig. 2(c)] are similar to those without flow [Fig. 2(a)]. These reflect the swimming speed distribution [26]. Hence, swimmers in aligned trajectories travel perpendicular to the flow at their swimming speed [but very slow swimmers cannot make much progress, biasing the distribution towards high speeds in Fig. 2(c)]. Without alignment [Fig. 2(b)], the speed distribution reflects contributions by swimming and the oscillatory flow, which accounts for the bias towards low speeds.

To statistically quantify observed alignment as a function of the flow parameters, we count trajectories with displacement $\Delta\mathbf{r}$ oriented perpendicular $N_\perp$ and parallel $N_\parallel$ to the flow direction and define $R = N_\perp/N_\parallel$. By parallel (perpendicular) displacements we mean swimming orientations within $\pm\pi/4$ of the flow (vorticity) axis. We also provide the alternative measure $r = [\langle\sin(\theta - \theta_{\text{flow}})\rangle^2 + \langle\cos(\theta - \theta_{\text{flow}})\rangle^2]^{1/2} \in [0,1]$, where averages are over all angles (which were doubled for axial distributions at resonance) [27]. Small r denotes isotropy, large r alignment (see Fig. 2). The

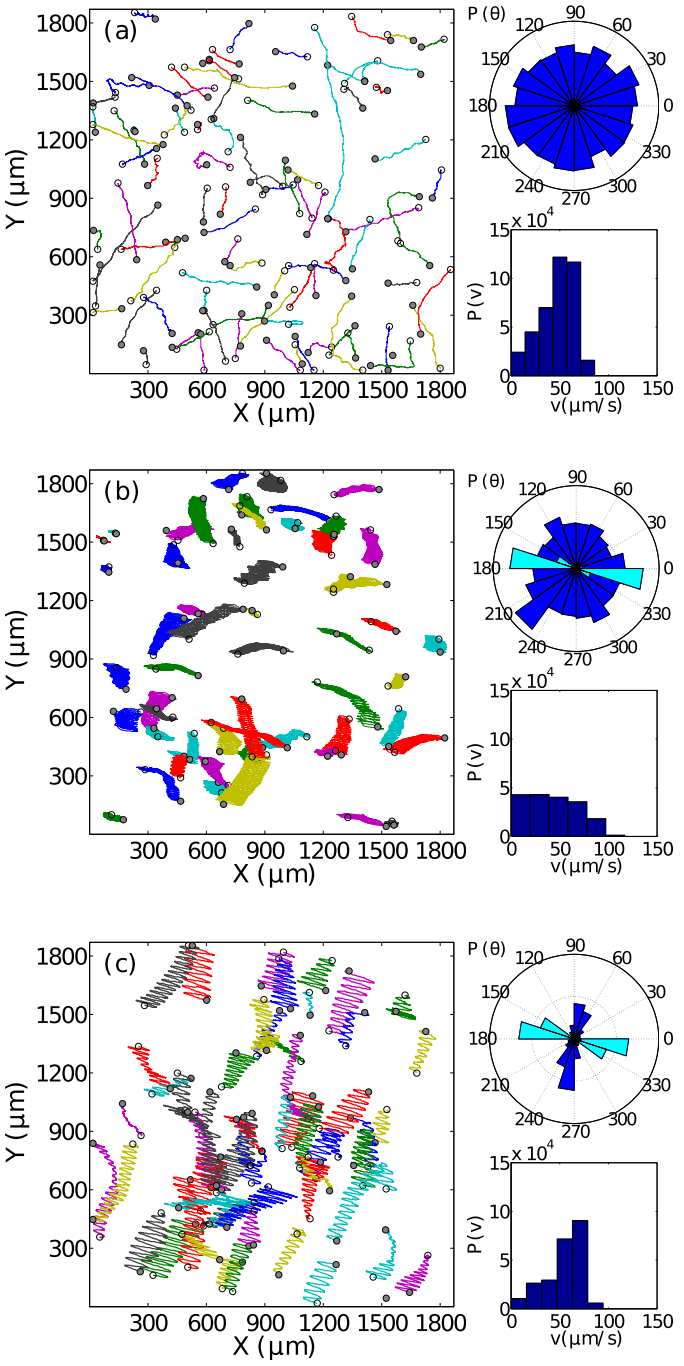

FIG. 2. Trajectories, orientation, and speed distributions of *D. salina*. (a) No flow: isotropic trajectories [alignment measures ($r = 0.02$ and $R = 0.9$); see the text]. (b) Oscillatory shear flow with amplitude $A = 240$ μm and frequency $f = 6$ Hz: Tracks show oscillation (cyan) at short times, but are isotropic (blue) at longer times ($r = 0.05$ and $R = 1.6$). (c) $A = 448$ μm and $f = 2$ Hz: Swimming directions align perpendicular (blue) to the flow oscillation direction (cyan) ($r = 0.53$ and $R = 4.4$). Open (closed) circles denote the start (end) points of each 2.5-s track.

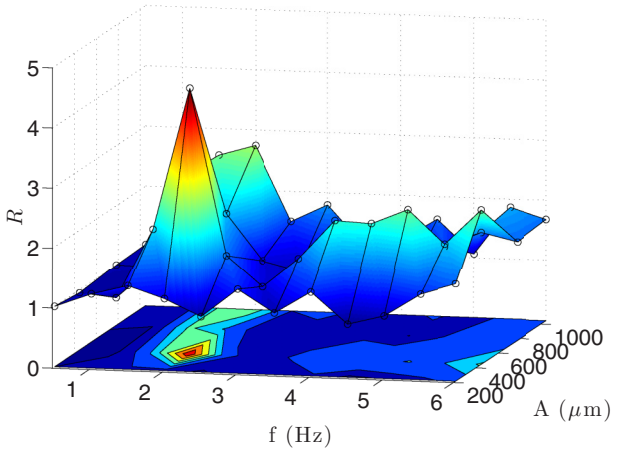

FIG. 3. Alignment ratio R as a function of driving amplitude A and frequency f for oscillatory flow in a shear cell with $H = 400$ μm gap width. Here A is a measure of horizontal displacement.

surface plot in Fig. 3 illustrates how the alignment has the characteristics of resonance, occupying a small region of the imposed flow parameter space. Fixed amplitude and frequency sections of the ordering surface are shown in Fig. 4 and discussed below.

Discussion. The observed trajectories result from the combination of shear flow and swimming. Many algae swim helically, in part to facilitate phototaxis via a directional eyespot [28]. Thus we model the algae as helical swimmers in a flow. Following [29], we assume that a cell at position $\mathbf{r}$ swimming with speed v in direction $\mathbf{p}$ has an intrinsic angular velocity $\omega_h\mathbf{n}$ about an axis $\mathbf{n}$, where $\mathbf{p}\cdot\mathbf{n} = \cos\beta$, for constant angle β, due to an asymmetric (nonplanar) flagellar stroke. Hence, if the only external torque is due to flow with velocity $\mathbf{u}$ and vorticity $\boldsymbol{\omega}$, spherical swimmers obey $\dot{\mathbf{r}} = \mathbf{u}(t) + v\mathbf{p}$, $\dot{\mathbf{p}} = [\frac{1}{2}\boldsymbol{\omega}(t) + \omega_h\mathbf{n}] \times \mathbf{p}$, and $\dot{\mathbf{n}} = \frac{1}{2}\boldsymbol{\omega}(t) \times \mathbf{n}$. Experimental observations suggest that the fluid velocity is $\mathbf{u}(t) = \dot{\gamma}_\infty Z\cos(\omega_d t)\mathbf{e}_x$, with vorticity $\boldsymbol{\omega}(t) = \dot{\gamma}_\infty\cos(\omega_d t)\mathbf{e}_y$. Here $\mathbf{e}_x$ and $\mathbf{e}_y$ are along the positive flow and vorticity directions, respectively, $\dot{\gamma}_\infty = \omega_d A/H$ is the maximum shear rate, and $\omega_d = 2\pi f$ is the angular driving frequency (recall that A, f, and H are driving amplitude, frequency, and gap width, respectively). Nondimensionalizing lengths with A and times with $1/\omega_d$, the model equations read

$$\dot{\mathbf{r}} = \Gamma\cos(t)Z\mathbf{e}_x + v\mathbf{p}, \tag{1}$$

$$\dot{\mathbf{p}} = \left[\frac{\Gamma}{2}\cos(t)\mathbf{e}_y + \Omega^{-1}\mathbf{n}\right] \times \mathbf{p}, \quad \dot{\mathbf{n}} = \frac{\Gamma}{2}\cos(t)\mathbf{e}_y \times \mathbf{n}, \tag{2}$$

where $\Gamma = \dot{\gamma}_\infty/\omega_d = A/H$ is the dimensionless shear rate, $\Omega = \omega_d/\omega_h$ is a frequency ratio, and $v = v/(A\omega_d) = v_0/(\Gamma\Omega)$ a nondimensional swimming speed, with $v_0 = v/(\omega_h H)$. The Cartesian representation of (1) and (2), with Z measured from the bottom plate and XY the flow-vorticity plane (Fig. 1), was solved numerically to simulate a suspension of swimmers (see [24]). The ratio R was computed from many simulations with a uniform distribution of initial swimmer orientations.

Nonswimmers ($v = 0$) passively follow the imposed oscillatory flow. In the absence of flow, the governing equations predict helical trajectories: $\mathbf{p}$ rotates around $\mathbf{n}$ (the helix axis) with frequency ω_h. With the experimental resonance close to helical swimming frequency, it is tempting to think that helical trajectories are responsible for the observed alignment. This is only partially true, as we shall see.

First we ask if the combination of nonhelical swimming and oscillatory shear alone is sufficient to induce ordering in experiment. Figure 4 displays the ordering ratio (experiment [Figs. 4(a) and 4(b)] and simulation [Figs. 4(c) and 4(d)]) and simulated swimmer trajectories [Fig. 4(e)] for a model

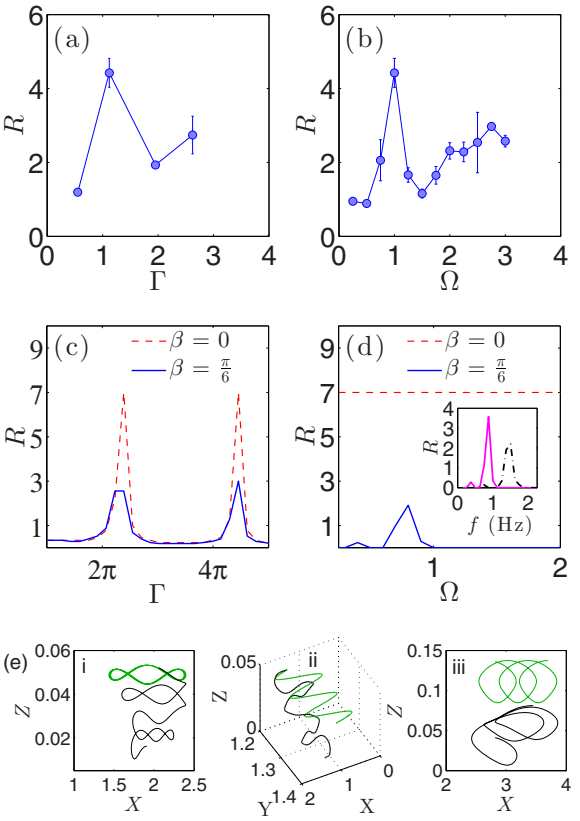

FIG. 4. Alignment ratio R vs amplitude Γ and frequency Ω from (a) and (b) experiment (error bars smaller than data points not shown) and (c) and (d) simulation. Simulation predictions are shown with ($\beta = \pi/6$, solid line) and without ($\beta = 0$, dashed line) helical swimming (frequency $f_h = 2$ Hz), only the latter providing frequency dependence. (e) Trajectories ($\beta = 0$, green line; $\beta = \pi/6$, black line) are also shown: (i) at resonance $[\Gamma,\Omega] = [7.5,0.75]$ for the XZ plane, (ii) 3D views, and (iii) off-resonance $[\Gamma,\Omega] = [4,0.75]$. Only trajectories closed in XZ provide ordering. The inset of (d) shows simulations of *P. piscida* in oscillatory flow, which increases its helical frequency from 1 (solid line) to 2 Hz (dash-dotted) when predating [30]. We predict a measurable shift in the resonance peak.

where helical swimming is switched off (dashed lines). While R peaks at characteristic values of the driving amplitude Γ [Fig. 4(c)], it is entirely independent of driving frequency [Fig. 4(d)] in stark contrast to the experiments. The nonhelical limit does, however, predict alignment: It is worth considering further. When $\beta = 0$, the governing equations simplify considerably if we choose Euler angles Θ and Φ [Fig. 1(c)] such that $\mathbf{p} = \mathbf{n} = (\sin\Theta\sin\Phi, \cos\Theta, \sin\Theta\cos\Phi)$, where Θ increases from the direction of vorticity $\mathbf{e}_y$ along the Y axis and Φ is measured from the Z axis [e.g., $(\Theta,\Phi) = (\pi/2,\pi/2)$ is along the X axis]. Equations (1) and (2) give

$$\dot{X} = v_\perp \sin\Phi + \Gamma\cos(t)Z, \tag{3}$$

$$\dot{Y} = v_\parallel, \tag{4}$$

$$\dot{Z} = v_\perp \cos\Phi, \tag{5}$$

$$\dot{\Theta} = 0, \quad \dot{\Phi} = \frac{\Gamma}{2}\cos(t), \tag{6}$$

where $\nu_\perp = \nu \sin\Theta_0$ and $\nu_\parallel = \nu \cos\Theta_0$ are the nondimensional swimming speed components perpendicular and parallel to $\mathbf{e}_y$. Integration of (4) and (6) yields $Y(t) = Y_0 + \nu_\parallel t$, $\Theta(t) = \Theta_0$, and

$$\Phi(t) = \Phi_0 + \frac{\Gamma}{2}\sin(t). \tag{7}$$

(Recall that $\Gamma = A/H$ is the nondimensional shear rate.) As the Y component of the trajectory grows linearly in time, independent of shear, alignment can only depend on the coupled X and Z dynamics. In particular, closed orbits in the XZ plane are present at resonance [see Fig. 4(e i)]. For such orbits, progress only in the Y direction is possible, leading to alignment. Off-resonance, orbits are open and cells can progress in the X and Z directions [Fig. 4(e ii)].

This phenomenology can be understood in terms of oscillatory Jeffery dynamics of the swimmer orientation. We see from (7) that oscillatory shear forces swimmer orientation in the vertical XZ plane to describe circular arcs swept sinusoidally in time (contrast this with circular Jeffery orbits in steady shear flow $\omega_d \to \infty$), with angular amplitude $\Gamma/2$. Folded orbits only arise when shear is sufficiently large to rotate swimmer orientation by integral multiples of π, so it can make no net progress during a cycle [see Fig. 4(e)]. This provides a prediction for the resonant ordering amplitude $\Gamma_{\text{res}} \approx 2\pi n$, $n \in \mathbb{Z}$, in good agreement with nonhelical simulations [Fig. 4(c)]. The latter agree qualitatively with the experimental results in Fig. 4(a). Quantitatively, much smaller values of Γ are sufficient to induce ordering in experiment. A possibility is that the Γ reported underestimates the shear rate swimmers were exposed to, e.g., because the intrinsic flagellar beats cause effective cell shape changes leading to unexpected response to shear [31,32]. Alternatively, additional mechanisms, such as those discussed below, may modify the ordering dynamics.

The model for nonhelical swimmers predicts alignment as a function of amplitude, but does not reproduce the experimentally observed dependence on both driving amplitude *and* frequency [Fig. 4(b)]. *D. salina* is a helical swimmer, rotating at 1.5–2 Hz [26]. This second, internal frequency provides the possibility of further resonance. Indeed, with $\beta \neq 0$ (recall that β is the angle between $\mathbf{p}$ and $\mathbf{n}$) numerical results reveal that ordering is frequency dependent [Fig. 4(d)]. Position equations are unchanged, but depend on more complex orientation dynamics resulting from the coupling of flow-induced and helical rotation. Cell orientation angles Θ_p and Φ_p, defining $\mathbf{p}$, evolve according to (see [24])

$$\dot{\Theta}_p = \Omega^{-1}\sin\Theta_n \sin(\Phi_n - \Phi_p), \tag{8}$$

$$\dot{\Phi}_p = \frac{\Gamma}{2}\cos(t) + \Omega^{-1}[\cos\Theta_n - \sin\Theta_n \cot\Theta_p \sin(\Phi_n + \Phi_p)], \tag{9}$$

whereas angles for $\mathbf{n}$ satisfy (6) such that $\dot{\Theta}_n = 0$ and $\dot{\Phi}_n = \Gamma\cos(t)/2$. As the $\mathbf{p}$ dynamics are slaved to the $\mathbf{n}$ dynamics, trajectories with helical swimming do retain broad features of nonhelical orbits in oscillatory shear [see Fig. 4(e)], but they are nevertheless qualitatively perturbed (even for infinitesimal β). Thus only for particular driving frequencies and amplitudes does helical swimming produce alignment-inducing orbits. The frequency condition for ordering can be obtained by considering the case of a swimmer with $\mathbf{n}$ in the direction of vorticity: $\Theta_n(0) = 0 = \Phi_n(0)$, $\Theta_p(0) = \beta$, and $\Phi_p(0) = 0$. Equation (9) then integrates to $\Phi_p(t) = \frac{\Gamma}{2}\sin(t) + \Omega^{-1}t$: A helical phase can perturb simple Jeffery rotation by the flow. Only when $\Omega \sim 1$, i.e., when the driving and helical phase are synchronized, can a resonant value of Γ give alignment, agreeing with both simulations and experiments [Figs. 4(b) and 4(d)].

Oscillatory Jeffery orbits and helical swimming provide a first-order explanation for the dependence of resonance in experiments on both frequency and amplitude. The model is predictive: Helical frequency shifts alter resonant alignment, e.g., simulations of the predatory dinoflagellate *Pfiesteria piscida* [24] predict a resonant frequency shift when helical frequency increases in the presence of prey [Fig. 4(d), inset]. This description could be extended to investigate how additional effects such as taxes, orientation noise, inertia, and cell shape dominate, compete, or act in concert

with helical swimming to affect resonance. Intriguing possibilities include stochastic resonance due to noise in the flow velocity gradients [33] and the aforementioned effective shape due to flagellar beats [31,32]. The possibility of flagellar deformation by shear [2] seems unlikely. Shear rates on the same order as our experiments can modify flagellar dynamics for cells held on a micropipette [34]. However, our cells are in suspension (free to rotate): Much larger shear will be necessary to deform their flagella. A full analytical investigation of the nonlinear dynamics of the helical model in oscillatory shear is beyond the scope of this paper, but it is clear that much is to be discovered, analogous to structures observed for swimming cells in Poiseuille flow [15].

Conclusion. We have demonstrated the surprising response of swimming microalgae to oscillatory shear flows, producing an alignment of trajectories with a set of resonance peaks in the parameter space of driving frequency and amplitude. A simple model combining shear and nonhelical swimming predicts resonant alignment of the trajectories of swimming cells, but only when helical swimming is included does the experimentally observed frequency dependence of the resonance arise. The rich dynamics and the counterintuitive interactions between swimmers and flow revealed by our experiments and modeling have implications for both active suspension rheology and the design of cell processing methods. While simplified models of swimmers (rod or spheroidal pushers and pullers with no helical motion) appear adequate to explain active rheological phenomena such as shear thickening in algal suspensions [17,35], the current work suggests such models may fail in active *oscillatory* rheology experiments. Biotechnologically, the results hint at methods for improvement in efficiency of the algal processing pipeline [36]. For example, in downstream processing of useful microalgae, like the β-carotene producer *D. salina*, cells commonly experience oscillatory flows. Resonant alignment will provide boundary accumulation over times L/v, where L is the size of the shear plate and v is the swimming speed. This may be engineered out by tuning process parameters from resonance or it may be fruitfully exploited as a way to guide and harvest cells.

Acknowledgments. We thank A. Schofield for providing colloids. O.A.C., W.C.K.P., M.D.H., and M.A.B. acknowledge support from the Carnegie Trust for the Universities of Scotland. O.A.C. further acknowledges support from the Winton Programme for the Physics of Sustainability and a Royal Society Research Grant; M.D.H. support from the Leverhulme Trust. O.A.C. and M.A.B. also acknowledge an EPSRC Mobility Grant (No. EP/J004847/1) and W.C.K.P. acknowledges the Programme Grant (No. EP/J007404/1) and ERC Advanced Grant (No. ERC-2013-AdG 340877-PHYSAPS).

[1] T. J. Pedley and J. O. Kessler, Hydrodynamic phenomena in suspensions of swimming microorganisms, Annu. Rev. Fluid Mech. **24**, 313 (1992).

[2] R. Rusconi and R. Stocker, Microbes in flow, Curr. Opin. Microbiol. **25**, 1 (2015).

[3] W. M. Durham, J. O. Kessler, and R. Stocker, Disruption of vertical motility by shear triggers formation of thin phytoplankton layers, Science **323**, 1067 (2009).

[4] M. A. Bees and O. A. Croze, Mathematics for streamlined biofuel production from unicellular algae, Biofuels **5**, 53 (2014).

[5] N. A. Hill and T. J. Pedley, Bioconvection, Fluid Dyn. Res. **37**, 1 (2005).

[6] R. N. Bearon, M. A. Bees, and O. A. Croze, Biased swimming cells do not disperse in pipes as tracers: a population model based on microscale behaviour, Phys. Fluids **24**, 121902 (2012).

[7] O. A. Croze, G. Sardina, M. Ahmed, M. A. Bees, and L. Brandt, Dispersion of swimming algae in laminar and turbulent channel flows: consequences for photobioreactors, J. R. Soc. Interface **10**, 20121041 (2013).

[8] W. M. Durham, E. Climent, M. Barry, F. D. Lillo, G. Boffetta, M. Cencini, and R. Stocker, Turbulence drives microscale patches of motile phytoplankton, Nat. Commun. **4**, 2148 (2013).

[9] C. Zhan, G. Sardina, E. Lushi, and L. Brandt, Accumulation of motile elongated micro-organisms in turbulence, J. Fluid Mech. **739**, 22 (2014).

[10] F. De Lillo, M. Cencini, W. M. Durham, M. Barry, R. Stocker, E. Climent, and G. Boffetta, Turbulent Fluid Acceleration Generates Clusters of Gyrotactic Microorganisms, Phys. Rev. Lett. **112**, 044502 (2014).
[11] O. A. Croze, E. E. Ashraf, and M. A. Bees, Sheared bioconvection in a horizontal tube, Phys. Biol. **7**, 046001 (2010).
[12] Y. Hwang and T. J. Pedley, Bioconvection under uniform shear: linear stability analysis, J. Fluid Mech. **738**, 522 (2014).
[13] X. Garcia, S. Rafaï, and P. Peyla, Light Control of the Flow of Phototactic Microswimmer Suspensions, Phys. Rev. Lett. **110**, 138106 (2013).
[14] C. R. Willams and M. A. Bees, Photo-gyrotactic bioconvection, J. Fluid Mech. **678**, 41 (2011).
[15] A. Zöttl and H. Stark, Nonlinear Dynamics of a Microswimmer in Poiseuille Flow, Phys. Rev. Lett. **108**, 218104 (2012).
[16] A. Sokolov and I. S. Aranson, Reduction of Viscosity in Suspension of Swimming Bacteria, Phys. Rev. Lett. **103**, 148101 (2009).
[17] S. Rafaï, L. Jibuti, and P. Peyla, Effective Viscosity of Microswimmer Suspensions, Phys. Rev. Lett. **104**, 098102 (2010).
[18] A. Chengala, M. Hondzo, and J. Sheng, Microalga propels along vorticity direction in a shear flow, Phys. Rev. E **87**, 052704 (2013).
[19] U. Pick, L. Karni, and M. Avron, Determination of ion content and ion fluxes in the halotolerant alga *Dunaliella salina*, Plant Physiol. **81**, 92 (1986).
[20] J. Polle (private communication).
[21] V. A. Martinez, R. Besseling, O. A. Croze, J. Tailleur, M. Reufer, J. Schwarz-Linek, L. G. Wilson, M. A. Bees, and W. C. Poon, Differential dynamic microscopy: A high-throughput method for characterizing the motility of microorganisms, Biophys. J. **103**, 1637 (2012).
[22] M. Kilfoil laboratory software research tools, available at http://people.umass.edu/kilfoil/downloads.html
[23] J. Crocker and D. G. Grier, Methods of digital video microscopy for colloidal studies, J. Colloid Interface Sci. **179**, 298 (1996).
[24] See Supplemental Material at http://link.aps.org/supplemental/10.1103/PhysRevFluids.1.051201 for further details about the simulations and experiments, including a video of swimmers in oscillatory shear showing resonant alignment.
[25] N. A. Hill and D.-P. Häder, A biased random walk model for the trajectories of swimming micro-organisms, J. Theor. Biol. **186**, 503 (1997).
[26] O. A. Croze, R. N. Bearon, and M. A. Bees, Gyrotactic swimmer dispersion in pipe flow: experimental challenge of competing models, arXiv:1608.08911.
[27] K. V. Mardia and P. Jupp, *Directional Statistics* (Wiley, New York, 2000).
[28] K. W. Foster and R. D. Smyth, Light antennas in phototactic algae, Microbiol. Rev. **44**, 572 (1980).
[29] R. N. Bearon, Helical swimming can provide robust upwards transport for gravitactic single-cell algae; a mechanistic model, J. Math. Biol. **66**, 1341 (2013).
[30] J. Sheng, E. Malkiel, J. Katz, J. Adolf, R. Belas, and A. R. Place, Digital holographic microscopy reveals prey-induced changes in swimming behavior of predatory dinoflagellates, Proc. Natl. Acad. Sci. USA **104**, 17512 (2007).
[31] S. O'Malley and M. A. Bees, The orientation of swimming biflagellates in shear flows, Bull. Math. Biol. **74**, 232 (2012).
[32] L. Jibuti, W. Zimmermann, S. Rafaï, and P. Peyla, Effective viscosity of active suspensions: Three-dimensional numerical modeling, arXiv:1412.3176.
[33] F. Guzmán-Lastra and R. Soto, Stochastic resonance on the transverse displacement of swimmers in an oscillatory shear flow, Phys. Rev. E **86**, 037301 (2012).
[34] G. S. Klindt, C. Ruloff, C. Wagner, and B. M. Friedrich, The load-response of the flagellar beat, arXiv:1606.00863.
[35] M. C. Marchetti, J. F. Joanny, T. B. Liverpool, J. Prost, M. Rao, and R. A. Simha, Hydrodynamics of soft active matter, Rev. Mod. Phys. **85**, 1143 (2013).
[36] S. A. Scott, M. P. Davey, J. S. Dennis, I. Horst, C. J. Howe, D. J. Lea-Smith, and A. G. Smith, Biodiesel from algae: challenges and prospects, Curr. Opin. Biotechnol. **21**, 277 (2010).